Site-specific quantitative analysis of cardiac mitochondrial protein phosphorylation

Maggie PY Lam[a,1], **Edward Lau**[a,1], **Sarah B Scruggs**[a], **Ding Wang**[a], **Tae-Young Kim**[a], **David A Liem**[a], **Jun Zhang**[a], **Christopher M Ryan**[b], **Kym F Faull**[b], and **Peipei Ping**[a,*]

[a]Departments of Physiology and Medicine, Division of Cardiology, David Geffen School of Medicine at UCLA, Los Angeles, CA 90095, USA

[b]The Pasarow Mass Spectrometry Laboratory, Department of Psychiatry and Biobehavioral Sciences and the Semel Institute for Neuroscience and Human Behavior, David Geffen School of Medicine at UCLA, Los Angeles, CA 90095, USA

Abstract

We report the development of a multiple-reaction monitoring (MRM) strategy specifically tailored to the detection and quantification of mitochondrial protein phosphorylation. We recently derived 68 MRM transitions specific to protein modifications in the respiratory chain, voltage-dependent anion channel, and adenine nucleotide translocase. Here, we have now expanded the total number of MRM transitions to 176 to cover proteins from the tricarboxylic acid cycle, pyruvate dehydrogenase complex, and branched-chain alpha-keto acid dehydrogenase complex. We utilized the transition set to analyze endogenous protein phosphorylation in human heart, mouse heart, and mouse liver. The data demonstrate the potential utility of the MRM workflow for studying the functional details of mitochondrial phosphorylation signaling.

Keywords

Multiple-reaction monitoring; mitochondria; phosphorylation; cardioprotection; quantification; cardiac biology

Introduction

Mitochondrial functions are continuously modulated by metabolic and signaling cues, including covalent protein modifications via reversible phosphorylation. Phosphorylation of pyruvate dehydrogenase (PDH) constitutes a classic metabolic switch that shunts pyruvate in or out of the glucose oxidation pathway [1, 2]. More recently, phosphorylation signaling was shown to modulate cardioprotection and ischemic injury through the reperfusion-injury salvage kinase (RISK) pathway [3, 4], and to serve as an allosteric regulator of respiratory chain complex activities [5, 6] and supercomplex assembly [7]. Large-scale proteomics

discovery experiments by our laboratory [8] and others [9, 10] have unveiled a complex network of hundreds of protein phosphorylation events in mitochondria. For example, the mitochondrial voltage-dependent anion channel (VDAC) and adenine nucleotide translocase (ANT) contain over 15 known phosphorylation sites, collectively targeted by multiple kinases including PKA, PKC, and GSK3β. The physiological functions of most of the recently discovered mitochondrial phosphorylations remain unknown.

Site-specific quantitative data on phosphorylation levels will help elucidate the functions of these novel phosphorylation modifications under various phenotypes, but technical challenges have hampered progress. Protein phosphorylation is reversible and transient, and frequently occurs at only partial stoichiometry, or occupancy, of the phosphoproteins. Phosphorylated peptides are thus more difficult to detect and quantify than unmodified peptides, and demand a combination of specialized enrichment methods and sensitive, specific mass spectrometric techniques [11, 12]. Recently, we developed a multiple-reaction monitoring (MRM) workflow to quantify mitochondrial protein phosphorylation [11]. In the workflow, peptide ion transitions were chosen that not only specifically identify phosphopeptides with high sensitivity, but also demarcate the locations of individual phosphorylations when multiple modifiable residues exist in close proximity. We optimized the MRM detection parameters for individual transitions, and utilized $RP-TiO_2-RP$ chromatography for phosphopeptide enrichment. In total, we manually collated over 60 parent ion/fragment ion transitions that unequivocally identify endogenous phosphorylation sites of interest. Isotope-labeled synthetic peptides corresponding to known phosphorylation sites were used as internal standards and assayed simultaneously with endogenous peptides to quantify the phosphopeptides in a site-specific manner.

In this study, we expanded the coverage of the MRM assays considerably and utilized them to analyze endogenous phosphorylations in mouse and human mitochondria. We observed unique phosphorylation patterns between species (mouse versus human), organs (heart versus liver), and metabolic states (fed versus fasted mice) that suggested differential regulation by phosphorylation in these systems. We further discuss some considerations for the development of phosphorylation-specific MRM transitions and their biological implications.

Materials and methods

Animals and human samples

Animal experiments were conducted in accordance with the Guide for the Care and Use of Laboratory Animals published by the National Research Council and approved by UCLA. C57BL/6 mice, 8-10 wk of age (Harlan Laboratories) were housed in a 12 h/12 h light-dark cycle with controlled temperature and humidity and free access to standard lab chow and water. For fasting experiments, food was withheld from three groups of two mice for 48 h before euthanasia. The control group had *ad libitum* access to food during the same period. Experimental procedures involving human tissues were approved by the UCLA Human Subjects Protection Committee and Institutional Review Board. Patients gave written informed consent. Anterior left ventricular wall samples were collected during heart transplantation from 3 individual heart failure patients between 05/05/2010 and 08/18/2010.

Mitochondrial protein isolation and digestion

Mitochondrial samples were isolated from the liver and heart of euthanized mice as previously described [13, 14]. Organs were excised, homogenized (Dounce homogenizer, 10 strokes for liver, 20 strokes for heart) in sucrose buffer (250 mmol·L^{-1} sucrose, 10 mmol·L^{-1} HEPES, 10 mmol·L^{-1} Tris-HCl, 1 mmol·L^{-1} EGTA, protease inhibitors (Roche Complete,

1x), phosphatase inhibitors (Sigma Phosphatase Inhibitor Cocktail II and III, 1x), and 10 mmol·L^{-1} dithiothreitol (Sigma), pH 7.5), then centrifuged (800 rcf, 4 °C, 7 min) to remove debris. The supernatant was re-centrifuged (4,000 rcf, 4 °C, 20 min). The pellets were washed, centrifuged again, then resuspended in 19% (v/v) Percoll (Sigma) in the sucrose buffer, overlaid on 30% and 60% Percoll, and centrifuged (12,000 rcf, 4 °C, 20 min). Purified mitochondria were collected from the bottom layer, washed twice, and pelleted (4,000 rcf, 4 °C, 20 min). The pellet was lysed by sonication in 10 mmol·L^{-1} Tris-HCl, pH 7.4. Protein concentration was assayed by the bicinchoninic acid procedure. Proteins were denatured (80 °C, 5 min) in 0.1% Rapigest (Waters), reduced and alkylated by dithiothreitol and iodoacetamide (Sigma), digested with 50:1 (w/w) sequencing-grade trypsin (Promega) (37 °C, overnight), treated with 0.1% trifluoroacetic acid (30 min), and centrifuged (14,000 rcf, ambient temperature, 15 min). Peptides from the supernatant were extracted by C18 spin columns (Thermo Pierce) according to the manufacturer's instructions.

Phosphopeptide enrichment and liquid chromatography

Peptide separation was carried out on an Agilent 1200 nano-LC system connected to an Agilent Phosphochip II HPLC-chip. The chip contained integrated microfluidics and a sandwiched Zorbax 300SB-C18 5-μm (RP)-TiO$_2$-RP trapping column connected to an analytical RP column. The binary buffer system consisted of buffer A (3% acetonitrile, 0.1% formic acid) and buffer B (97% acetonitrile, 0.1% formic acid). Phosphopeptides from the trapping column were eluted with 16 μL of Phosphochip elution buffer (Agilent). Peptide separation on the analytical column was accomplished by ramping buffer B% (0 min, 3%; 70 min, 45%) at a flow-rate of 300 nL·min^{-1}.

Multiple-reaction monitoring

Transitions were monitored on an Agilent 6460 triple-quadrupole mass spectrometer equipped with a ChipCube ion source as described [11]. Collision energies for each transition were chosen after ramping from 0 to 50 V at 4-V intervals using the *Optimizer for Peptides* software (Agilent). Fragmentor voltage was similarly optimized by ramping from 50 to 200 V. Dwell time ranged from 50 to 300 ms to cover at least 8 data points per LC peak. For endogenous peptide analysis, 4 μg of mitochondrial digests were co-injected with 1 pmol each of crude synthetic unmodified peptides and 20 to 200 fmol each of crude synthetic phosphorylated peptides (Thermo PEPotec SRM).

Data analysis

All chromatograms were inspected manually using the *Mass Hunter Qualitative Analysis* software. Areas under MRM peaks were integrated at full-width prior to smoothing.

Results and Discussion

We previously reported 62 MRM transitions for quantifying mitochondrial phosphorylation [11]. In this study, we expanded the number of developed MRM transitions to a total of 176, corresponding to 54 phosphorylated mitochondrial peptides and their unmodified counterparts (Table 1). The new MRM assay covers additional phosphorylation sites in ANT, the tricarboxylic acid cycle proteins, the PDH complex, and the branched-chain alpha-keto acid dehydrogenase (BCKDH) complex, that have been previously discovered in large-scale experiments [8, 10]. They complement the mitochondrial phosphorylation coverage of the previously described MRM transitions for ANT, VDAC, and respiratory chain proteins [11]. The MRM transitions were optimized using synthetic heavy-isotope-labeled standards of unmodified and phosphorylated peptides (Fig. 1A-B). From replicate injections, the newly-determined transitions were found to have a median coefficients of variation (CV) of 9.7% in peak areas (interquartile range: 6.3% to 20.0%). Eighty-five of the 114 novel

transitions had CV of <20%, which would suggest that the majority of transitions afforded highly reproducible responses in the mass spectrometer. Furthermore, the determination of light-to-heavy peak area ratios is expected to be significantly more precise than absolute area calculations [15], since factors that may influence absolute peak areas would identically alter the co-eluting endogenous and labeled peptides.

The endogenous protein phosphorylation sites in human and mouse samples were then analyzed with the derived transitions. Figures 1C-J show the heavy (synthetic) and light (endogenous) signals from 8 phosphorylation sites in 5 proteins found in the human cardiac mitochondria. Each of these sites was only partially phosphorylated, since their unmodified counterparts were also detected in the human heart (Supplementary Figure S1). Four other phosphopeptides, from ANT isoform 4, fumarate hydratase, and 2-oxoglutarate dehydrogenase were previously reported in discovery experiments, but were below the limit of detection in the experiments reported here. The corresponding unmodified peptides were readily detected, suggesting the peptide sequences may be monitored in principle (Supplementary Figure S2). It is possible that these reported sites were only transiently occupied by phosphate, or were not phosphorylated under basal conditions in the human heart.

Certain phosphopeptides contain multiple potential phosphorylation sites that may be modified in any one of several distinct combinations. This complexity necessitated judicious selection of MRM transitions in order to unequivocally identify the phosphorylated residues. The PDH E1 alpha subunit (PDHA1) peptide YHGHSMSDPGVSYR contains both the well-studied pS293 and pS300, in addition to another serine and two tyrosine residues that are potential sites of phosphorylation. The two serine sites at S293 and S300 give rise to potentially four different permutations, of which three were analyzed (unmodified, pS293, pS293+pS300). We optimized four and six transitions for the pS293 singly-phosphorylated and the pS293+pS300 doubly-phosphorylated peptide, respectively (Fig. 1C-D, 3A). In the pS293 singly-phosphorylated peptide, the phosphate-containing b_8^{2+} ion and the unmodified y_6^{2+} ion distinguished the presence of phosphorylation between S293 and S300. In the doubly-phosphorylated peptide, the unmodified b_2 ion and the b_5–$H_3PO_4^{2+}$ ion demarcated one phosphorylation modification to be between G291 and S293, whereas the unmodified y_2^{2+} and the modified y_6^{2+} specified another phosphorylation that exists between P297 and S300. Since S293 and S300 were the only modifiable residues within the two regions, the transitions identified a population of doubly-phosphorylated PDHA1 at the two sites.

Phosphorylation in human and mouse cardiac mitochondria

Using the devised transitions, we observed evidence for differential phosphorylation between human and mouse cardiac mitochondria samples. For instance, the human ANT1 pT84 phosphopeptide signal was on average ≈2.5 times more intense than that in C57BL/6 mice (average light-to-heavy area ratios 2.07 versus 0.81; p = 0.04, Student's t test; n = 3), whereas the unmodified peptides showed no significant difference between the two species (average light-to-heavy area ratios 1.06 versus 0.97; p = 0.88; n = 3) (Figure 2A). Given that the light-to-heavy ratios of both the phosphorylated and unmodified peptides and the injection amount of the synthetic standards (1 pmol unmodified peptide versus 100 fmol phosphopeptide) were known, the occupancy of the phosphorylation site could be calculated in principle. The quantity of the phosphopeptide is given by the light-to-heavy area ratios of the phosphorylated peptides multiplied by the amount of the heavy phosphopeptide standard injected. The occupancy is then given by the quantity of the phosphopeptide divided by the sum of the quantities of the phosphopeptide and the corresponding native peptide. As an example, if we were to assume the crude synthetic peptides have identical purity, our result would put the range of ANT1 T84 phosphorylation occupancy to be 19.0% in human heart and 8.8% in mouse heart. Precise quantification of occupancy, however, will require the use

of high-purity synthetic standards. In addition to pT84, we also observed that the pY191 phosphorylation signal in ANT1 was more intense in the human heart compared to the mouse heart (e.g. in Figures 1I and 2B). These results demonstrate that MRM assays could be used to monitor potential changes in endogenous phosphorylations in disease in a site-specific and quantitative manner.

Phosphorylation in mouse liver and heart mitochondria

We next utilized the MRM assays to analyze endogenous protein phosphorylations in the mouse heart and the mouse liver. Cardiac and hepatic mitochondria contain proteins encoded from the same genome, but nevertheless contrast in functions, proteome compositions, and disease manifestation. The molecular basis of such inter-organ variances is complex, with reversible phosphorylation known to constitute one crucial post-translational signature of organ phenotypes [9]. The membrane transporters VDAC and ANT were selected for these inter-organ comparisons. For three residues (S22, T84, Y191) located at the cytoplasmic-side lumen of ANT, S22 and Y191 phosphorylations were detectable in the heart but not in the liver (Fig. 2B), whereas the pT84 phosphopeptide was conspicuously more abundant in the heart (data not shown). Though we do not rule out miniscule phosphorylations in the liver that existed below detection limits or with other modifications, these data corroborate spectral-count measurements which suggested ANT1 is phosphorylated most abundantly in the heart but minimally in the liver [9]. In contrast, when VDAC was compared using transitions previously shown to specifically identify the pS117 phosphorylation [11], similar phosphopeptide levels were found in both organs (Fig. 2C). The contrasts are intriguing as VDAC and ANT play crucial roles in mitochondrial permeability transition, a phenomenon with considerable organ differences in manifestation. Y191 in particular forms a tyrosine ladder with the proximal Y187 and Y195 at the lumen that may regulate ANT conductance in the heart [16, 17]. Both Y191 and Y195 phosphorylation have been reported in the heart and in the brain, but their presence and stoichiometry in other organs has not been investigated. The tyrosine ladder residues are known to be hypo-phosphorylated under cardiac ischemia, which would imply phosphorylation in this region has an important role in preserving cardiac function [17]. However, the lack of phosphorylated tyrosine ladder residues in liver mitochondria would suggest that phosphorylation is not obligatory for basal translocase activity. Organ-specific phosphorylation profiles could provide a potential regulatory principle given the dissimilar ATP synthesis in hepatic and cardiac mitochondria. We speculate that future experimentation will illuminate whether phosphorylation at critical junctions of permeability-associated proteins may influence apoptotic signaling.

Phosphorylation profiles in fasted mouse heart and liver

Lastly, we examined the well-studied PDHA1 phosphorylation in the heart and the liver in a mouse 48-hr fasting model. Mitochondrial PDH is a key metabolic protein that regulates metabolite influx into the TCA cycle. Phosphorylation rapidly and reversibly regulates the activities of PDH enzymatic complexes at S232, S293, and S300. Increased phosphorylation at these sites deactivates enzymatic activities, potentially to reduce ROS production and promote glycolysis when cellular conditions do not favor glucose oxidation. In our experiments, the doubly-phosphorylated (pS293 and pS300) peptide behaved differently from the singly-phosphorylated (pS293) peptide following fasting, supporting the idea that further regulatory details may be learned from combinatorial site-specific profiles. In the liver and to a lesser degree the heart, the pS293-only singly-phosphorylated peptide remained largely unchanged, whereas the doubly-phosphorylated population increased following fasting (Fig. 3B).

Fasting is predicted to elicit an acute metabolic response where the heart and the liver would preserve glucose for brain consumption. Increases in PDH phosphorylation levels were thus not unexpected. It was less clear how the detailed phosphorylation patterns in the regulatory sites would alter, i.e., whether individual phosphorylation sites would vary in response in different organs. The PDH kinase isoforms (PDK1-4) exhibit high degrees of redundancy, wherein all four PDK isoforms could phosphorylate S293 to inactivate PDH during starvation. The phosphorylation of pS300, mainly by PDK4, is thought to introduce a hierarchical gate-keeper control by protecting pS293 from dephosphorylation. Our finding that the pS293+pS300 double phosphorylation is differentially regulated from the pS293 site may have implications for the gate-keeping model, and whether the pS300 site serves additional regulatory functions. Measurements of individual pS293 and pS300 levels would be confounded by the nuances of potential connectivity.

In the current study, we have purposefully limited the scope of the analysis to relative quantification between identical peptides across samples due to the varied purities of the crude synthetic peptides (Thermo PEPotec). We were nevertheless able to infer changes in occupancy on sites whose phosphorylation patterns were conspicuously altered or where differential protein expression was not a cause for concern. It is important to stress that the presented technique is completely translatable to absolute quantification experiments with little to no modifications. Assuming no other post-translational modifications exist at the local peptide sequence, the abundance of the phosphorylated and the unmodified peptides will add up to the protein abundance. Absolute site occupancy could then be measured through high-purity synthetic peptide standards with known concentrations (e.g. Thermo AQUA), or calculated through crude synthetic peptides if the protein abundance ratio between two samples is known, e.g., by using an additional, proteotypic peptide standard for an unmodified sequence.

Targeted quantification of phosphorylation sites is most commonly studied using immunobiological techniques, radioactive ^{32}P labeling, and mutagenesis. MRM offers several advantages for quantifying protein phosphorylation [18, 19]. For instance, the safety of stable isotopes over radioisotopes facilitates widespread applications. Moreover, MRM assays in combination with stable-isotope-labeled synthetic peptide standards are highly multiplexed and allow for hundreds of targeted phosphopeptides to be studied virtually simultaneously. By comparing the absolute quantity of phosphorylated and unphosphorylated peptides, the absolute levels of occupancy and comparisons of phosphorylation degrees between multiple sites are possible. The connectivity of two proximal phosphorylated residues can also be taken into consideration without requiring a large multiplicity of custom antibodies, as in the case of PDHA1 pS293 and pS300. Lastly, MRM assays afford excellent sensitivity. Contemporary LC/triple-quadrupole instruments operating in MRM mode could reach the detection limit of 20 amol (1.2×10^7 molecules) of analytes when optimized. In the experiments reported here, 4 μg of digested mitochondrial proteins were injected on-column. Assuming a mammalian mitochondrion has a dry mass of $\approx 1.1 \times 10^{-13}$ g [20], a detection limit of less than one phosphopeptide molecule per mitochondrion is theoretically achievable. However, currently obstacles remain in the adoption of MRM methods as each phosphorylation site of interest must be individually tailored to its own specific transition information, then optimized and validated. An initial method development phase therefore exists before a phosphorylation site can be assayed in biological samples. Further, the peptide sequences to be analyzed are restricted by the locations of the phosphorylation sites of interest. Certain peptides containing chemical modifications such as oxidized methionine or deamidated asparagine are unavoidable and may interfere with absolute quantitation. Nevertheless, it has been noted that the phosphorylated and unmodified peptides may be chemically modified to the same extent and thus will not hinder stoichiometric occupancy calculations [21]. These interfering chemical

modifications can be further controlled by additional transitions that accommodate the resulting mass shifts and the use of pre-modified synthetic standards.

In summary, we devised 108 novel MRM transitions and utilized them to examine protein phosphorylations in VDAC, ANT, and PDH. Inter-specific differences between mouse and human cardiac mitochondria have been observed, as well as intra-genomic variations between the heart and the liver. In a mouse 48-hr fasting model, the doubly-phosphorylated (pS293 and pS300) peptide in PDHA1 behaved distinctly from the singly-phosphorylated (pS293) peptide, suggesting regulatory details may be learned from combinatorial site-specific profiles. Our data demonstrate the utility of MRM to unlock phosphorylation signaling in cardiac mitochondria. Importantly, the assays are easily translatable by other researchers to studies in multiple tissues and models.

Supplementary Material

Refer to Web version on PubMed Central for supplementary material.

Acknowledgments

References

1. Holness MJ, Sugden MC. Regulation of pyruvate dehydrogenase complex activity by reversible phosphorylation. Biochem Soc Trans. 2003; 31:1143–51. [PubMed: 14641014]

2. Hue L, Taegtmeyer H. The Randle cycle revisited: a new head for an old hat. Am J Physiol Endocrinol Metab. 2009; 297:E578–91. [PubMed: 19531645]

3. Murphy E, Steenbergen C. Mechanisms underlying acute protection from cardiac ischemia-reperfusion injury. Physiol Rev. 2008; 88:581–609. [PubMed: 18391174]

4. Miura T, Tanno M, Sato T. Mitochondrial kinase signalling pathways in myocardial protection from ischaemia/reperfusion-induced necrosis. Cardiovasc Res. 2010; 88:7–15. [PubMed: 20562423]

5. Acin-Perez R, Gatti DL, Bai Y, Manfredi G. Protein phosphorylation and prevention of cytochrome oxidase inhibition by ATP: coupled mechanisms of energy metabolism regulation. Cell Metab. 2011; 13:712–9. [PubMed: 21641552]

6. Acin-Perez R, Salazar E, Kamenetsky M, Buck J, Levin LR, Manfredi G. Cyclic AMP produced inside mitochondria regulates oxidative phosphorylation. Cell Metab. 2009; 9:265–76. [PubMed: 19254571]

7. Kane LA, Youngman MJ, Jensen RE, Van Eyk JE. Phosphorylation of the F(1)F(o) ATP synthase beta subunit functional and structural consequences assessed in a model system. Circ Res. 2010; 106:504–U41. [PubMed: 20035080]

8. Deng N, Zhang J, Zong CG, Wang YJ, Lu HJ, Yang PY, Wang WH, Young GW, Wang YB, Korge P, Lotz C, Doran P, Liem DA, Apweiler R, Weiss JN, Duan HL, Ping PP. Phosphoproteome analysis reveals regulatory sites in major pathways of cardiac mitochondria. Molecular & cellular proteomics : MCP. 2011; 10:1–14.

9. Huttlin EL, Jedrychowski MP, Elias JE, Goswami T, Rad R, Beausoleil SA, Villen J, Haas W, Sowa ME, Gygi SP. A tissue-specific atlas of mouse protein phosphorylation and expression. Cell. 2010; 143:1174–89. [PubMed: 21183079]

10. Hornbeck PV, Kornhauser JM, Tkachev S, Zhang B, Skrzypek E, Murray B, Latham V, Sullivan M. PhosphoSitePlus: a comprehensive resource for investigating the structure and function of experimentally determined post-translational modifications in man and mouse. Nucleic acids research. 2012; 40:D261–70. [PubMed: 22135298]

11. Lam MPY, Scruggs SB, Kim TY, Zong C, Lau E, Wang D, Ryan CM, Faull KF, Ping P. An MRM-based workflow for quantifying cardiac mitochondrial protein phosphorylation in murine and human tissue. J Proteomics. 2012

12. Olsen JV, Vermeulen M, Santamaria A, Kumar C, Miller ML, Jensen LJ, Gnad F, Cox J, Jensen TS, Nigg EA, Brunak S, Mann M. Quantitative phosphoproteomics reveals widespread full phosphorylation site occupancy during mitosis. Science signaling. 2010; 3:ra3. [PubMed: 20068231]

13. Lau E, Wang D, Zhang J, Yu H, Lam MP, Liang X, Zong N, Kim TY, Ping P. Substrate- and isoform-specific proteome stability in normal and stressed cardiac mitochondria. Circ Res. 2012; 110:1174–8. [PubMed: 22456183]

14. Zhang J, Li X, Mueller M, Wang Y, Zong C, Deng N, Vondriska TM, Liem DA, Yang JI, Korge P, Honda H, Weiss JN, Apweiler R, Ping P. Systematic characterization of the murine mitochondrial proteome using functionally validated cardiac mitochondria. Proteomics. 2008; 8:1564–75. [PubMed: 18348319]

15. Kuzyk MA, Smith D, Yang J, Cross TJ, Jackson AM, Hardie DB, Anderson NL, Borchers CH. Multiple reaction monitoring-based, multiplexed, absolute quantitation of 45 proteins in human plasma. Molecular & cellular proteomics : MCP. 2009; 8:1860–77.

16. Feng J, Lucchinetti E, Enkavi G, Wang Y, Gehrig P, Roschitzki B, Schaub MC, Tajkhorshid E, Zaugg K, Zaugg M. Tyrosine phosphorylation by Src within the cavity of the adenine nucleotide translocase 1 regulates ADP/ATP exchange in mitochondria. American journal of physiology Cell physiology. 2010; 298:C740–8. [PubMed: 20007455]

17. Feng J, Zhu M, Schaub MC, Gehrig P, Roschitzki B, Lucchinetti E, Zaugg M. Phosphoproteome analysis of isoflurane-protected heart mitochondria: phosphorylation of adenine nucleotide translocator-1 on Tyr194 regulates mitochondrial function. Cardiovasc Res. 2008; 80:20–9. [PubMed: 18558627]

18. Picotti P, Aebersold R. Selected reaction monitoring-based proteomics: workflows, potential, pitfalls and future directions. Nature methods. 2012; 9:555–66. [PubMed: 22669653]

19. Domanski D, Murphy LC, Borchers CH. Assay development for the determination of phosphorylation stoichiometry using multiple reaction monitoring methods with and without phosphatase treatment: application to breast cancer signaling pathways. Analytical chemistry. 2010; 82:5610–20. [PubMed: 20524616]

20. Bahr GF, Zeitler E. Study of mitochondria in rat liver. Quantitative electron microscopy. The Journal of cell biology. 1962; 15:489–501. [PubMed: 13968987]

21. Atrih A, Turnock D, Sellar G, Thompson A, Feuerstein G, Ferguson MA, Huang JT. Stoichiometric quantification of Akt phosphorylation using LC-MS/MS. J Proteome Res. 2010; 9:743–51. [PubMed: 19902931]

Highlights

- We developed 100+ MRM transitions for mitochondrial phosphorylation quantification

- Phosphorylation stoichiometry differed between species, organs, and metabolic states

- In pyruvate dehydrogenase, connectivity exists between adjacent phosphorylation sites
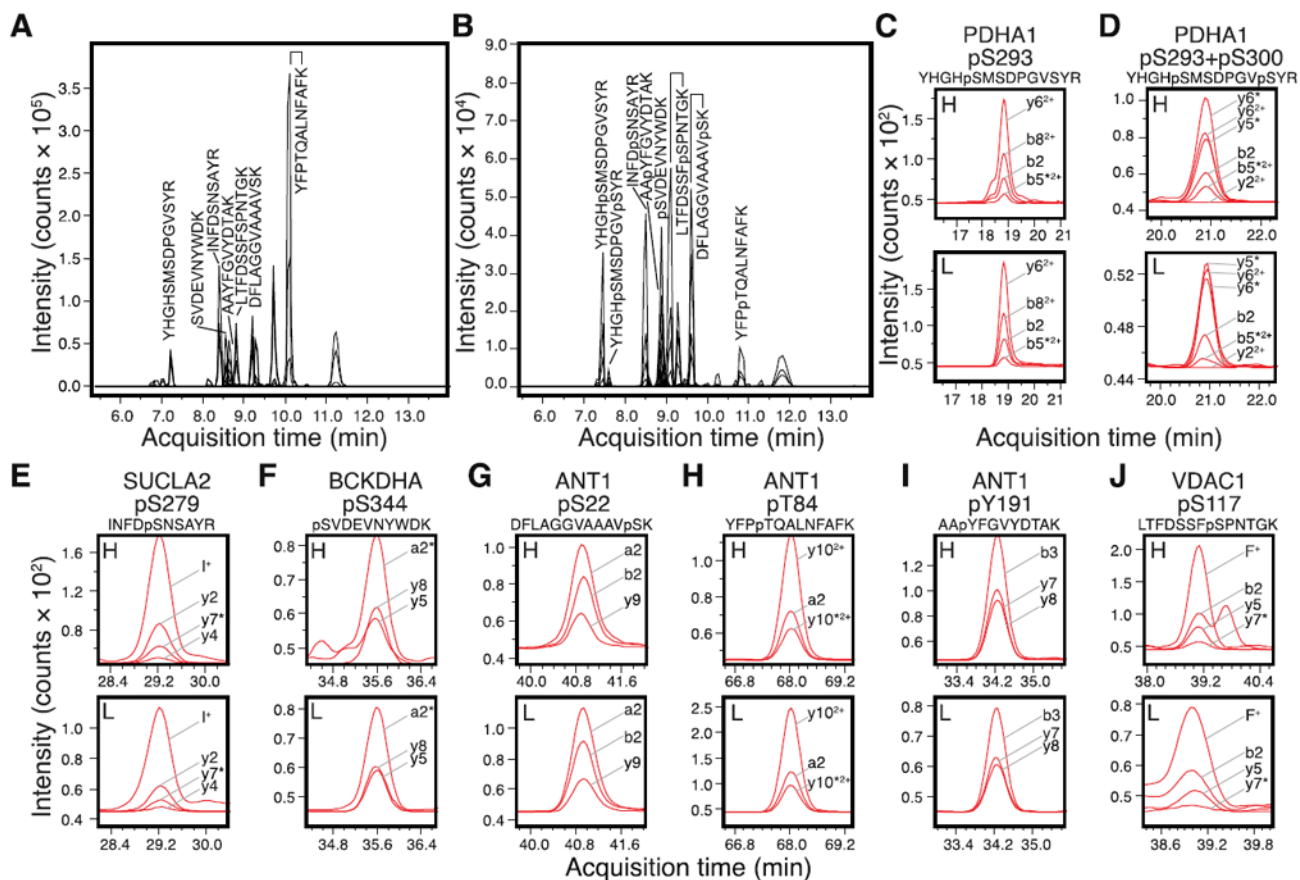
Figure 1. MRM transitions and quantitative analysis of endogenous human mitochondrial phosphorylations

The new set of MRM assays were validated using heavy-isotope-labeled synthetic peptide standards of **(A)** unmodified peptides and **(B)** their respective phosphorylated versions. The peaks corresponding to peptides from PDH, VDAC, ANT, shown in C-J, are labeled with their sequences in the chromatogram. **(C-J)** Human protein phosphorylation was detected by comparing the heavy-labeled standard (H) and unlabeled endogenous peptides (L). The MRM signals for a panel of transitions are shown and labeled; asterisks next to the fragment ions denote neutral loss of H_3PO_4. **(C)** Pyruvate dehydrgeonase E1 complex alpha subunit (PDHA1) pS293 phosphopeptide YHGHpSMSDPGVSYR. **(D)** PDHA1 pS293+pS300 doubly-phosphorylated peptide YHGHpSMSDPGVpSYR. **(E)** Succinyl-CoA ligase [ADP-forming] subunit beta (SUCLA2) pS279 phosphopeptide INFDpSNSAYR. **(F)** Branched-chain alpha-keto acid dehydrogenase subunit alpha (BCKDHA) pS344 phosphopeptide pSVDEVNYWDK. **(G)** Adenine nucleotide translocase 1 (ANT1) pS22 phosphopeptide DFLAGGVAAAVpSK. **(H)** ANT1 pT84 phosphopeptide YFPpTQALNFAFK. **(I)** ANT1 pY191 phosphopeptide AApYFGVYDTAK. **(J)** Voltage-dependent anion channel I (VDAC1) pS117 phosphopeptide LTFDSSFpSPNTGK. For consistency, amino acid residue numbering is based on mouse homolog sequence in Uniprot [19].
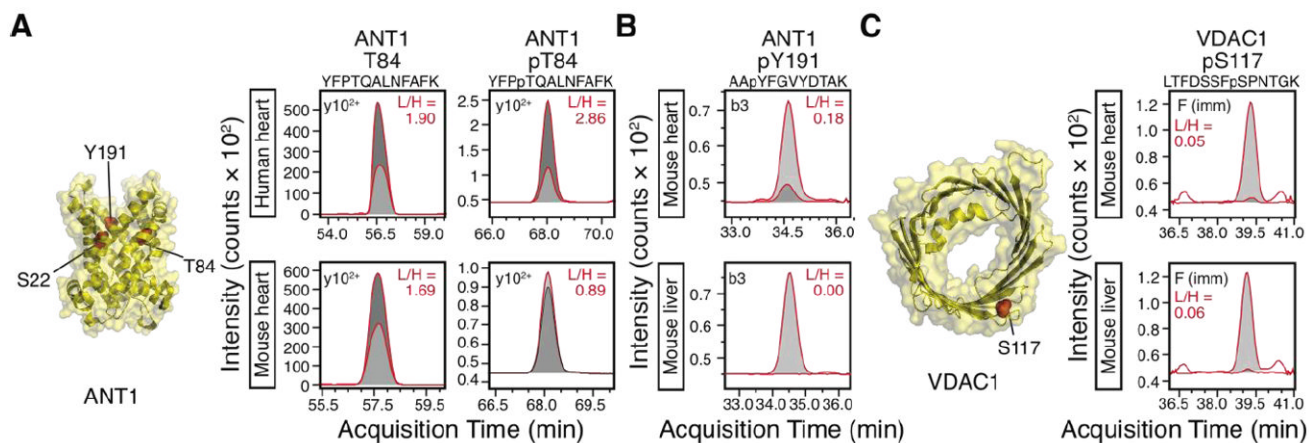
Figure 2. Phosphorylation differences between species and organs
(A) The adenine nucleotide translocase 1 (ANT1) phosphopeptide at T84 was approximately 3 times higher in a human heart sample than in the mouse, whereas the unmodified peptide was insignificantly different. A representative MRM transition is shown to illustrate the difference in areas between the heavy (synthetic; light gray) and light (endogenous; dark gray) peptides. In the actual area ratio calculation, the summed areas of all MRM transitions for each peptide were used. **(B)** ANT1 Y191 was detectable in the heart but not the liver. A representative MRM transition (b3 ion) is shown. **(C)** Voltage-dependent anion channel 1 (VDAC1) phosphorylation at the potential GSK3β target S117 was comparable in both organs. A representative MRM transition (phenylalanine immonium ion) is shown.
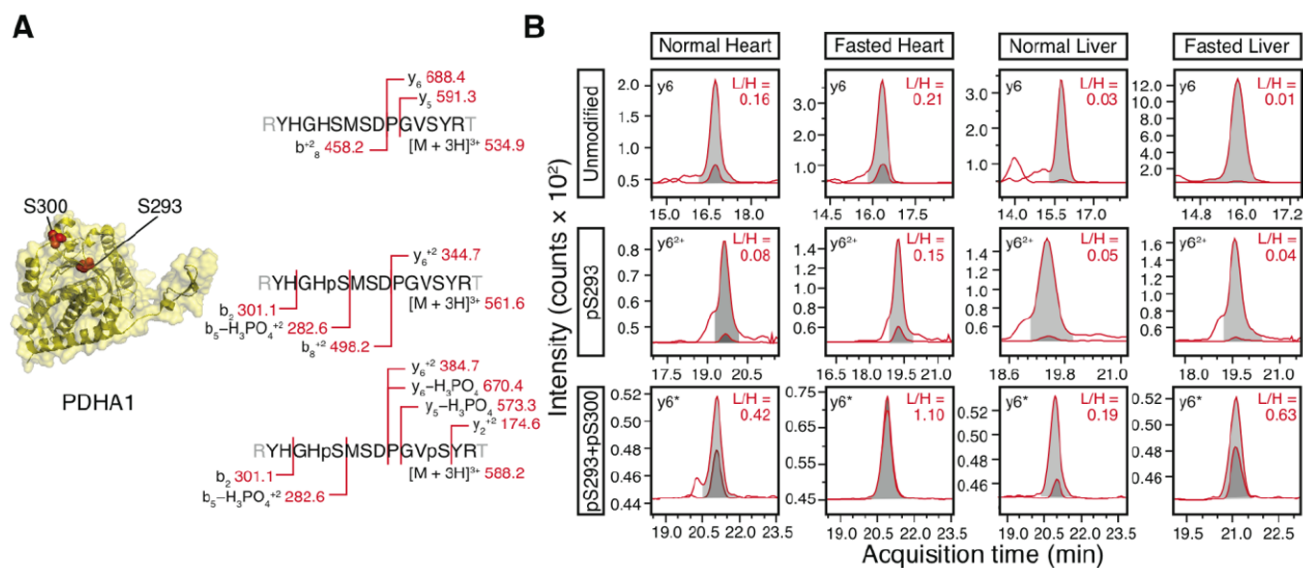
Figure 3. Changes in PDH phosphorylation levels at pS293 and pS300 following fasting
(A) Scheme of the MRM transitions for the unmodified peptide spanning the two residues, the singly-phosphorylated peptide modified at S293, and the doubly-phosphorylated peptide modified at S293 and S300. The mass-to-charge ratios for identifying the heavy isotope-labeled peptide standards were shown. **(B)** Following fasting, the pS293+pS300 double phosphorylation was up-regulated in the heart and the liver. The integrated area of the heavy reference peptide (light gray) and the endogenous peptide (dark gray) are shown. Only one representative MRM transition is illustrated. For the unmodified peptide, the y6 fragment ions are shown. For the pS293 singly-phosphorylated peptide, the $y6^{2+}$ fragment ions are shown. For the pS293/pS300, the $y6-H_3PO_4$ (denoted by y6*) fragment ions are shown. In the actual area ratio calculation, the summed areas of all MRM transitions for each peptide were used.

Table 1

List of derived MRM transitions for mitochondrial phosphopeptides and their corresponding unmodified peptide.

Peptide Sequence (heavy-labeled)	Protein Name	Species	Modified residue(s)	Precursor ion m/z	z	Product ion m/z	Fragment identity	a Frag (V)	b CE (V)	c CV (%)
AApYFGVYDTAK	ANT1 (ADP/ATP translocase 1)	d M, e H		647.3	2+	908.5	y8	180	16	7.1
		M, H	Y191	647.3	2+	761.4	y7	180	20	8.6
		M, H		647.3	2+	386.1	b3	180	20	6.9
DFLAGGIAAAVpSK	ANT1 (ADP/ATP translocase 1)	M		654.3	2+	861.4	y9	155	12	3.2
		M	S22	654.3	2+	834.5	y10-H_3PO_4	155	24	0.7
		M		654.3	2+	263.1	b2	155	20	7.7
		M		654.3	2+	235.1	a2	155	36	7.9
DFLAGGVAAAVpSK	ANT1 (ADP/ATP translocase 1)	H		647.3	2+	847.4	y9	165	12	8.1
		H	S22	647.3	2+	263.1	b2	165	20	6.8
		H		647.3	2+	235.1	a2	165	36	9.7
YFPpTQALNFAFK	ANT1 (ADP/ATP translocase 1)	M, H		767.9	2+	612.8	$y10^{2+}$	215	20	0.1
		M, H	T84	767.9	2+	563.8	y10-$H_3PO_4$$^{2+}$	215	20	4.5
		M, H		767.9	2+	283.1	a2	215	28	0.6
GpTGGALVLVLYDK	ANT4 (ADP/ATP translocase 4)	M, H		697.4	2+	758.5	y6	120	24	24.9
		M, H	T293	697.4	2+	648.4	M-H_3PO_4	120	12	29.1
		M, H		697.4	2+	326.1	b5-H_3PO_4	120	20	37.8
pSVDEVNYWDK	BCKDHA (2-oxoisovalerate dehydrogenase subunit alpha)	M, H		671.8	2+	1076.5	y8	130	16	6.9
		M, H	S344	671.8	2+	733.3	y5	130	16	3.2
		M, H		671.8	2+	141.1	a2-H_3PO_4	130	36	0.7
SGLGELILPENEPGpSIMPGK	FH (Fumarate hydratase)	M, H		1107.0	2+	720.3	y6	250	40	37.8
		M, H	S363	1107.0	2+	670.4	b7	250	40	50.4
		M, H		1107.0	2+	309.2	y3	250	40	62.4
MAGpSAWVSK	IDH3A (Isocitrate dehydrogenase [NADP], cytoplasmic)	M		512.7	2+	795.4	y8-H_3PO_4	130	16	9.4
		M	S4	512.7	2+	724.4	y7-H_3PO_4	130	12	6.2

Peptide Sequence (heavy-labeled)	Protein Name	Species	Modified residue(s)	Precursor ion m/z	z	Product ion m/z	Fragment identity	a Frag (V)	b CE (V)	c CV (%)
SpSLATMAHAQSLVEAQPNVDK	OGDH (2-oxoglutarate dehydrogenase)	M		512.7	2+	242.2	y2	130	24	21.7
		M		762.4	3+	1050.5	$y20\text{-}H_3PO_4^{2+}$	160	24	27.5
		M	S103	762.4	3+	729.7	$M\text{-}H_3PO_4^{3+}$	160	12	26.8
		M		762.4	3+	580.3	y5	160	24	23.3
		M		762.4	3+	270.1	$b3\text{-}H_3PO_4$	160	36	20.8
GpSLAAVAHAQSLVEAQPNVDK	OGDH (2-oxoglutarate dehydrogenase)	H		731.7	3+	908.5	y8	160	16	12.6
		H	S103	731.7	3+	807.9	$y15^{2+}$	160	8	14.7
		H		731.7	3+	580.3	y5	160	20	14.3
VVNAPIFHVNSDDPEAVMpYVCK	OGDH (2-oxoglutarate dehydrogenase)	M, H		864.7	3+	1105.0	$y18^{2+}$	190	20	35.3
		M, H	Y485	864.7	3+	592.8	$y9^{2+}$	190	20	34.9
		M, H		864.7	3+	199.2	b2	190	24	55.7
		M, H		864.7	3+	171.2	a2	190	44	52.0
YHGHpSMSDPGVSYR	PDHA1 (Pyruvate dehydrogenase E1 component subunit alpha, somatic form)	M, H		561.6	3+	498.2	$b8^{2+}$	130	8	10.1
		M, H	S293	561.6	3+	344.7	$y6^{2+}$	130	12	9.7
		M, H		561.6	3+	301.1	b2	130	24	7.9
		M, H		561.6	3+	282.6	$b5\text{-}H_3PO_4^{2+}$	130	24	8.5
YHGHpSMSDPGVpSYR	PDHA1 (Pyruvate dehydrogenase E1 component subunit alpha, somatic form)	M, H	S293/S300	588.2	3+	670.4	$y6\text{-}H_3PO_4$	130	20	10.4
		M, H		588.2	3+	573.3	$y5\text{-}H_3PO_4$	130	24	7.9
		M, H		588.2	3+	384.7	$y6^{2+}$	130	12	3.1
		M, H		588.2	3+	301.1	b2	130	32	5.7
		M, H		588.2	3+	282.6	$b5\text{-}H_3PO_4^{2+}$	130	24	11.2
		M, H		588.2	3+	174.6	$y2^{2+}$	130	16	28.3
GGSMHHMpYGK	PDHA1 (Pyruvate dehydrogenase E1 component subunit alpha, testis-specific form)	M		528.2	2+	586.2	y4	130	20	19.0
		M	Y157	528.2	2+	455.2	y3	130	20	29.4
		M		528.2	2+	212.1	y2	130	32	3.0
INFDpSNSAYR	SUCLA2 (Succinyl-CoA ligase [ADP-forming], subunit beta)	M, H	S279	638.8	2+	804.4	$y7\text{-}H_3PO_4$	130	24	15.7

Peptide Sequence (heavy-labeled)	Protein Name	Species	Modified residue(s)	Precursor ion m/z	z	Product ion m/z	Fragment identity	a Frag (V)	b CE (V)	c CV (%)
		M, H		638.8	2+	506.3	y4	130	24	13.0
		M, H		638.8	2+	228.2	y2	130	16	10.9
		M, H		638.8	2+	86.1	I immonium	130	32	10.8
LTFDSSFpSPNTGK	VDAC1 (Voltage-dependent anion-selective channel protein 1)	M, H	S117	744.8	2+	740.4	y7-H_3PO_4	215	28	8.6
		M, H		744.8	2+	524.3	y5	215	28	7.6
		M, H		744.8	2+	215.1	b2	215	24	7.0
		M, H		744.8	2+	120.1	F immonium	215	50	9.2
CTTDHISAAGPWLK	ACO2 (Aconitate hydratase)	M, H	Unmodified	522.3	3+	837.5	y8	130	12	5.9
		M, H		522.3	3+	608.4	y5	130	16	7.5
		M, H		522.3	3+	155.8	y1	130	32	7.7
AAYFGVYDTAK	ANT1 (ADP/ATP translocase 1)	M, H	Unmodified	607.3	2+	1071.5	y9	135	12	5.4
		M, H		607.3	2+	908.5	y8	135	16	7.5
		M, H		607.3	2+	761.4	y7	135	12	5.4
DFLAGGVAAAVSK	ANT1 (ADP/ATP translocase 1)	H	Unmodified	607.3	2+	838.5	y10	160	12	9.5
		H		607.3	2+	263.1	b2	160	16	9.1
		H		607.3	2+	235.1	a2	160	32	9.9
YFPTQALNFAFK	ANT1 (ADP/ATP translocase 1)	M, H	Unmodified	727.9	2+	818.5	y7	185	24	27.4
		M, H		727.9	2+	572.8	y10²⁺	185	20	25.2
		M, H		727.9	2+	283.1	a2	185	24	23.0
GTGGALVLVLYDK	ANT4 (ADP/ATP translocase 4)	M, H	Unmodified	657.4	2+	970.6	y8	165	16	0.5
		M, H		657.4	2+	857.5	y7	165	16	1.1
		M, H		657.4	2+	758.5	y6	165	16	6.0
SVDEVNYWDK	BCKDHA (2-oxoisovalerate dehydrogenase subunit alpha)	M, H	Unmodified	631.8	2+	1076.5	y8	130	16	9.7
		M, H		631.8	2+	187.1	b2	130	12	13.5
		M, H		631.8	2+	159.1	a2	130	28	14.9
AMLDPEGILNPYK	D2HGDH (D-2-hydroxyglutarate dehydrogenase)	M	Unmodified	734.9	2+	1038.6	y9	160	20	15.4
		M		734.9	2+	203.1	b2	160	24	14.0

Peptide Sequence (heavy-labeled)	Protein Name	Species	Modified residue(s)	Precursor ion m/z	z	Product ion m/z	Fragment identity	a Frag (V)	b CE (V)	c CV (%)
GILNPYK	D2HGDH (D-2-hydroxyglutarate dehydrogenase)	M		734.9	2+	175.1	a2	160	32	14.1
		M, H	Unmodified	406.7	2+	642.4	y5	100	4	16.3
		M, H		406.7	2+	415.2	y3	100	12	11.0
		M, H		406.7	2+	171.1	b2	100	4	6.9
SGLGELILPENEPGSSIMPGK	FH (Fumarate hydratase)	M, H		1067.1	2+	1350.7	y13	190	32	38.8
		M, H	Unmodified	1067.1	2+	670.4	b7	190	36	33.4
		M, H		1067.1	2+	309.2	y3	190	36	30.9
MAGSAWVSK	IDH3A (Isocitrate dehydrogenase [NADP], cytoplasmic)	M		472.7	2+	813.5	y8	100	8	10.6
		M	Unmodified	472.7	2+	742.4	y7	100	8	20.9
		M		472.7	2+	175.1	a2	100	12	21.6
GYDSDNPRVR	MUTA (Methylmalonyl-CoA mutase)	M, H		594.8	2+	427.2	$y7^{2+}$	130	8	22.5
		M, H	Unmodified	594.8	2+	336.1	b3	130	28	18.8
		M, H		594.8	2+	185.1	y1	130	32	20.4
SSLATMAHAQSLVEAQPNVDK	OGDH (2-oxoglutarate dehydrogenase)	M		735.7	3+	908.5	y8	160	16	5.7
		M	Unmodified	735.7	3+	779.4	y7	160	16	9.6
		M		735.7	3+	580.3	y5	160	20	7.9
GSLAAVAHAQSLVEAQPNVDK	OGDH (2-oxoglutarate dehydrogenase)	H		705.0	3+	908.5	y8	130	16	8.3
		H	Unmodified	705.0	3+	779.4	y7	130	12	11.5
		H		705.0	3+	580.3	y5	130	12	10.0
VVNAPIFHVNSDDPEAVMYYCK	OGDH (2-oxoglutarate dehydrogenase)	M, H		838.0	3+	1157.5	$y20^{2+}$	160	20	0.0
		M, H	Unmodified	838.0	3+	1065	$y18^{2+}$	160	20	0.0
		M, H		838.0	3+	552.8	y9	160	20	1.1
IEQLSPFPFDLLLK	OGDH (2-oxoglutarate dehydrogenase)	M, H		834.5	2+	1297.8	y11	160	28	3.1
		M, H	Unmodified	834.5	2+	1097.7	y9	160	20	3.7
		M, H		834.5	2+	371.2	b3	160	24	7.1
YHGHSMSDPGVSYR	PDHA1 (Pyruvate dehydrogenase E1 component subunit alpha, somatic form)	M, H		534.9	3+	688.4	y6	130	16	4.0
		M, H	Unmodified	534.9	3+	591.3	y5	130	16	2.6

NIH-PA Author Manuscript NIH-PA Author Manuscript NIH-PA Author Manuscript

Peptide Sequence (heavy-labeled)	Protein Name	Species	Modified residue(s)	Precursor ion m/z	z	Product ion m/z	Fragment identity	a Frag (V)	b CE (V)	c CV (%)
		M, H		534.9	3+	458.2	b8²⁺	130	8	4.4
GGSMHMYGK	PDHA1 (Pyruvate dehydrogenase E1 component subunit alpha, somatic form)	M	Unmodified	488.2	2+	506.3	y4	130	16	17.1
		M		488.2	2+	375.2	y3	130	16	20.8
		M		488.2	2+	202.1	b3	130	16	20.3
INFDSNSAYR	SUCLA2 (Succinyl-CoA ligase [ADP- forming], subunit beta)	M, H		598.8	2+	969.5	y8	130	16	9.2
		M, H	Unmodified	598.8	2+	822.4	y7	130	20	8.2
		M, H		598.8	2+	228.2	b2	130	16	10.4
LTFDSSFSPNTGK	VDAC1 (Voltage-dependent anion-selective channel protein 1)	M, H		704.8	2+	845.4	y8	180	20	1.8
		M, H	Unmodified	704.8	2+	524.3	y5	180	28	0.9
		M, H		704.8	2+	215.1	b2	180	20	0.9

All transitions verified for each listed peptide are shown. Amino acid residue numbering is based on the mouse homolog sequence in Uniprot.

[a] Frag (V): fragmentor voltage

[b] CE (V): collision energy

[c] CV: coefficient of variation. Coefficients of variation were calculated from three repeated injections, with the exception of the ANT1 pT84 and OGDH unmodified Y485 peptides, which were based on duplicate injections.

[d] M: the listed peptide corresponds to mouse protein sequence

[e] H: the listed peptide corresponds to human protein sequence